Lattice Boltzmann model for incompressible flows through porous media

Zhaoli Guo*
National Laboratory of Coal Combustion, Huazhong University of Science and Technology, Wuhan 430074, China

T. S. Zhao
Department of Mechanical Engineering, The Hong Kong University of Science and Technology, Hong Kong, China
(Received 6 May 2002; published 17 September 2002)

In this paper a lattice Boltzmann model is proposed for isothermal incompressible flow in porous media. The key point is to include the porosity into the equilibrium distribution, and add a force term to the evolution equation to account for the linear and nonlinear drag forces of the medium (the Darcy's term and the Forcheimer's term). Through the Chapman-Enskog procedure, the generalized Navier-Stokes equations for incompressible flow in porous media are derived from the present lattice Boltzmann model. The generalized two-dimensional Poiseuille flow, Couette flow, and lid-driven cavity flow are simulated using the present model. It is found the numerical results agree well with the analytical and/or the finite-difference solutions.

DOI: 10.1103/PhysRevE.66.036304 PACS number(s): 47.55.Mh, 47.11.+j

I. INTRODUCTION

Transport phenomena in a porous medium arise in many fields of science and engineering. In the past several decades, flow in porous media has been studied both experimentally and theoretically. Flow in porous media usually involves three scales: the pore scale, the representative elementary volume (REV) scale, and the domain scale. The REV is defined as a minimum element at which scale characteristics of a porous flow holds. The REV scale is much larger than the pore scale but is much smaller than the domain scale. In classical studies, flow in porous media is usually modeled by some semiempirical models due to the complex structure of a porous medium based on the volume-averaging at the REV scale. Several widely used models have been introduced in the literature, such as the Darcy, the Brinkman-extended Darcy, and the Forchheimer-extended Darcy models. A recent achievement in modeling flow in porous media is the so-called generalized model, in which all fluid forces and the solid drag force are considered in the momentum equation [1–3]. The Darcy and the two extended models (Brinkman and Forchheimer) mentioned above can be viewed as the limiting cases of the generalized model. Furthermore, due to its similarity with the Navier-Stokes equations, this model can be used to solve transient flow in porous media. Due to the complexity of the flows in porous media, analytical solutions are difficult to obtain except for very few problems. For general cases, only approximate solutions can be obtained numerically. Many numerical simulations have been conducted in the past using conventional schemes based on discretizations of the semiempirical models [3–8].

The lattice Boltzmann method (LBM), a new method for simulating fluid flow and modeling physics in fluids, has also been successfully applied to flow in porous media [9]. Two approaches have been adopted in simulations of porous flow using LBM. In the first approach, the fluid in the pores of the medium is directly modeled by the standard LBM. It is well known that unlike the conventional numerical methods based on discretizations of macroscopic continuum equations, LBM is based on microscopic models and mesoscopic kinetic equations for fluids. The kinetic nature of LBM enables it very suitable for fluid systems involving microscopic interactions. Furthermore, the simple bounce-back rule for no-slip boundary condition makes it very suitable to simulate the fluid flows in porous media. In fact, the lattice gas automata (LGA) method, the ancestor of LBM, was already applied to study the flows in porous media early in 1980s [10,11], and LBM was applied to porous flow soon after its emergence in 1989 [12]. Later studies confirmed the reliability of LBM in modeling fluid flow in porous media [12–18]. In these studies, the fluid is modeled by the standard lattice Boltzmann equation (LBE), and the interaction between the fluid and solid is handled with the no-slip bounce-back rule. This is the most straightforward way to apply LBM to porous flows. The main advantage of this method is that detailed local information of the flow can be obtained, which can be used to study macroscopic relations. However, the method at the pore scale needs detailed geometric information, and the size of computation domain cannot be too large due to limited computer resources since each pore of the medium should contains several lattice nodes. For a large flow domain, the method may perhaps be unusable. Another disadvantage associated with this approach is that the superficial (i.e., the volume-averaged) velocity of the flow cannot be high. It is known that the volume-averaged velocity of the flow $\overline{u} \sim \epsilon u_f$, where u_f and $\overline{u}$ refer to the pure and averaged velocity of the fluid, respectively, and ϵ is the porosity of the medium. As applied the standard LBM to the interstitial fluid in the pores of the medium, the fluid velocity cannot be too high due to the low Mach number limit for LBM, and thus $\overline{\mathbf{u}}$ cannot be high, either, especially for a medium of low porosity.

An alternative approach to apply LBM to porous flow is to model the fluid at the REV scale. This is accomplished by including an additional term to the standard LBE to account for the presence of a porous medium. For instance, Dardis and McCloskey proposed a lattice Boltzmann model by in-

*Electronic address: pcihust@wuhan.cngb.com

troducing a term describing the no-slip boundary condition [19]. Spaid and Phelan proposed a model (referred to as SP) based on the Brinkman equation for single-component flow in porous media [20]. Freed proposed a similar model by adding a force term to model flows through a resistance field [21]. The SP model was later extended for multicomponent system by combining this model with a multicomponent LB algorithm [22]. Recently, Martys improved the SP model by introducing an effective viscosity in the Brinkman equation, and the accuracy and stability are also improved [23]. The SP model and improved versions have been proved to be a simple and a computationally efficient method to model flows in porous media. In this approach, the detailed structure of the medium is ignored, and the statistical properties of the medium are included into the model directly. Therefore, the detailed flow information at the pore scale is often unavailable. However, this approach can be used for systems of large size; and with appropriate models for the porous medium, the LBM can produce reasonable results. However, although the Brinkman model has been widely used to describe flows in porous media, some limitations still exist in this model. As pointed by Vafai and Kim [24], without a convective term, there is no mechanism for the development of the flow field, and this will lead to a physically flawed and unrealistic situation. The nonlinear inertial term is not included in the Brinkman model either, and thus, is suitable for low-speed flows only.

In this paper, we will propose a generalized lattice Boltzmann model for incompressible flows in porous media with the linear and nonlinear matrix drag components as well as the inertial and viscous forces taken into account. In this model, the inertial force is included based on a recently developed technique [25], and the equilibrium distribution function is modified to account for the porosity of the medium. The model is applicable for a medium with both a constant and a variable porosity, and can be used to transient flows. Through the Chapmann-Enskog expansion, the generalized Navier-Stokes equations for flow in porous media can be derived from the model in the incompressible limit. Numerical simulations of the generalized two-dimensional (2D) Poiseuille flow, Couette flow, and lid-driven cavity flow are carried out. It is found that the LBM results agree well with the analytical and/or the finite-difference solutions.

II. GENERALIZED MODEL FOR POROUS FLOW

The generalized model for isothermal incompressible fluid flow in porous media was proposed by several groups. In this work we take the form proposed by Nithiarasu *et al.* [3], which is applicable for a medium with both a constant and a variable porosity. The model can be expressed by the following generalized Navier-Stokes equation:

$$\nabla \cdot \mathbf{u} = 0, \tag{1a}$$

$$\frac{\partial \mathbf{u}}{\partial t} + (\mathbf{u} \cdot \nabla)\left(\frac{\mathbf{u}}{\epsilon}\right) = -\frac{1}{\rho}\nabla(\epsilon p) + \nu_e \nabla^2 \mathbf{u} + \mathbf{F}, \tag{1b}$$

where ρ is the fluid density, $\mathbf{u}$ and p the volume-averaged velocity and pressure, respectively, and ν_e an effective parameter. $\mathbf{F}$ represents the total body force due to the presence of a porous medium and other external force fields, and is given by

$$\mathbf{F} = -\frac{\epsilon \nu}{K}\mathbf{u} - \frac{\epsilon F_\epsilon}{\sqrt{K}}|\mathbf{u}|\mathbf{u} + \epsilon \mathbf{G}, \tag{2}$$

where ν is the shear viscosity of the fluid that is not necessarily the same as ν_e. G is the body force induced by an external force. The geometric function F_ϵ and the permeability K of the porous medium are related to the porosity ϵ based on Ergun's experimental investigations [26], and can be expressed as [27]

$$F_\epsilon = \frac{1.75}{\sqrt{150\epsilon^3}}, \tag{3}$$

$$K = \frac{\epsilon^3 d_p^2}{150(1-\epsilon)^2}, \tag{4}$$

where d_p is the solid particle diameter. One can see that as $\epsilon \to 1$, i.e., in the absence of porous medium, the generalized momentum equation (1b) reduces to the Navier-Stokes equation for free fluid flows. The second term on the right side of Eq. (1b) is the Brinkman term accounting for the presence of a solid boundary. The boundary layer may be very thin in some problems, but its inclusion is important, especially for flows involving mass and/or heat transfer. The first and the second terms on the right side of Eq. (2) are the linear (Darcy) and nonlinear (Forchheimer) drags due to the porous medium. The quadratic nature of the nonlinear resistance makes it negligible for low-speed flows, but is more noteworthy in hindering the fluid motion for high-speed flows. Without this nonlinear term, Eq. (1b) becomes the Brinkman-extended Darcy equation.

The flow governed by Eq. (1) is characterized by the porosity ϵ and three nondimensional parameters: the Reynolds number Re, the Darcy number Da, and the viscosity ratio J, as, respectively, defined as

$$\mathrm{Re} = \frac{LU}{\nu}, \quad \mathrm{Da} = \frac{K}{L^2}, \quad J = \frac{\nu_e}{\nu}, \tag{5}$$

where L and U are the characteristic length and velocity, respectively. For a given medium, the ratio between the linear and the nonlinear drags is about

$$\frac{F_\epsilon |\mathbf{u}| / \sqrt{K}}{\nu/K} \sim \sqrt{\mathrm{Da}}\mathrm{Re}. \tag{6}$$

Therefore, for the cases in which the Reynolds number or the Darcy number is small, the nonlinear drag can be neglected, and the general model reduces to the Brinkman-extended Darcy model. On the other hand, for large Re or Da, however, the nonlinear drag must be considered.

III. LATTICE BOLTZMANN MODEL FOR THE GENERALIZED NAVIER-STOKES EQUATIONS

The LBM originates from the lattice-gas automata method, and can also be viewed as a special discrete scheme for the Boltzmann equation with discrete velocities. In LBM, the fluid is modeled by a single-particle distribution function (DF). The evolution of the DF is governed by a lattice Boltzmann equation:

$$f_i(\mathbf{x}+\mathbf{e}_i\delta_t,t+\delta_t)-f_i(\mathbf{x},t)=-\frac{f_i(\mathbf{x},t)-f_i^{(eq)}(\mathbf{x},t)}{\tau}, \quad (7)$$

where $f_i(\mathbf{x},t)$ is the DF for the particle with velocity $\mathbf{e}_i$ at position $\mathbf{x}$ and time t, δ_t is the time increment. τ is the nondimensional relaxation time and $f_i^{(eq)}$ is the equilibrium distribution function (EDF). The EDF must be defined appropriately such that the mass and momentum are conserved and some symmetry requirements are satisfied in order to describe the correct hydrodynamics of the fluid. For example, in the *DnQb* [28] models, the EDF is defined by

$$f_i^{(eq)}=\omega_i\rho\left[1+\frac{\mathbf{e}\cdot\mathbf{u}}{c_s^2}+\frac{\mathbf{uu}:(\mathbf{e}_i\mathbf{e}_i-c_s^2\mathbf{I})}{2c_s^4}\right], \quad (8)$$

where ω_i is the weight and c_s is the sound speed. Both ω_i and c_s depend on the underlying lattice. For the $D2Q9$ model, the discrete velocities are given by $\mathbf{e_0}=\mathbf{0}$, and $\mathbf{e}_i=\lambda_i(\cos\theta_i,\sin\theta_i)c$ with $\lambda_i=1$, $\theta_i=(i-1)\pi/2$ for $i=1$–4, and $\lambda_i=\sqrt{2}$, $\theta_i=(i-5)\pi/2+\pi/4$ for $i=5$–8. Here $c=\delta_x/\delta_t$ and δ_x is the lattice spacing. The weights are given by $\omega_0=4/9$, $\omega_i=1/9$ for $i=1$–4, $\omega_i=1/36$ for $i=5$–8, and $c_s=c/\sqrt{3}$. In LBM, the fluid density ρ and velocity $\mathbf{u}$ are defined by the DFs, i.e., $\rho=\Sigma_i f_i$, $\rho\mathbf{u}=\Sigma_i\mathbf{e}_i f_i$. It can be shown that the Navier-Stokes equations can be derived from the LBE (7) through a Chapman-Enskog expansion procedure in the incompressible limit.

To model incompressible fluid flow in a porous medium governed by the above generalized equations in the LBM framework, we first propose a LBE for a medium with porosity ϵ, but the linear and nonlinear drag effects of the medium as well as the external force are neglected temporally (i.e., $\mathbf{F}=\mathbf{0}$). The LBE reads

$$\overline{f_i}(\mathbf{x}+\mathbf{e}_i\delta_t,t+\delta_t)-\overline{f_i}(\mathbf{x},t)=-\frac{\overline{f_i}(\mathbf{x},t)-\overline{f_i}^{(eq)}(\mathbf{x},t)}{\tau}, \quad (9)$$

where $\overline{f_i}(\mathbf{x},t)$ and $\overline{f_i}^{(eq)}$ are the volume-averaged DF and EDF at the REV scale, respectively. Note that the averaging is only of conceptual significance, just as what is done in the standard LBE where the averaged particle number (or the distribution function) is used to replace the Boolen number in LGA. No averaging is needed in practical simulations. In what follows, the overbars will be omitted for the sake of convenience. To include the effect of the porous medium, the EDF is now defined as

$$f_i^{(eq)}=\omega_i\rho\left[1+\frac{\mathbf{e}\cdot\mathbf{u}}{c_s^2}+\frac{\mathbf{uu}:(\mathbf{e}_i\mathbf{e}_i-c_s^2\mathbf{I})}{2\epsilon c_s^4}\right]. \quad (10)$$

As in the standard LBM, the volume-average fluid density ρ and velocity $\mathbf{u}$ are defined by the volume-averaged DFs,

$$\rho=\sum_i f_i, \quad \rho\mathbf{u}=\sum_i \mathbf{e}_i f_i. \quad (11)$$

Through the Chapman-Enskog procedure, we can obtain the following macroscopic equations from the LBE (9) in the limit of small Mach number (see the Appendix for details):

$$\frac{\partial\rho}{\partial t}+\nabla\cdot(\rho\mathbf{u})=0, \quad (12a)$$

$$\frac{\partial(\rho\mathbf{u})}{\partial t}+\nabla\cdot\left(\frac{\rho\mathbf{uu}}{\epsilon}\right)=-\nabla(\epsilon p)+\nabla\cdot[\rho\nu_e(\nabla\mathbf{u}+\mathbf{u}\nabla)], \quad (12b)$$

where $p=c_s^2\rho/\epsilon$ and $\nu_e=c_s^2(\tau-0.5)\delta_t$. If $\rho\approx\rho_0=\text{const}$, the above equations reduce to the generalized Navier-Stokes equation (1) with $\mathbf{F}=\mathbf{0}$.

For general cases where $\mathbf{F}\neq 0$, the LBE must be modified to account for the total force. This is done by adding a force term into the LBE,

$$f_i(\mathbf{x}+\mathbf{e}_i\delta_t,t+\delta_t)-f_i(\mathbf{x},t)=-\frac{f_i(x,t)-f_i^{(eq)}(x,t)}{\tau}+\delta_t F_i. \quad (13)$$

Recently it is shown that in order to obtain correct equations of hydrodynamics, the force term F_i must be chosen appropriately and the fluid velocity must be redefined [25]. A suitable choice for flow in porous media governed by Eq. (1) is to take

$$F_i=\omega_i\rho\left(1-\frac{1}{2\tau}\right)\left[\frac{\mathbf{e}_i\cdot\mathbf{F}}{c_s^2}+\frac{\mathbf{uF}:(\mathbf{e}_i\mathbf{e}_i-c_s^2\mathbf{I})}{\epsilon c_s^4}\right]. \quad (14)$$

Accordingly, the fluid velocity is defined as

$$\rho\mathbf{u}=\sum_i \mathbf{e}_i f_i+\frac{\delta_t}{2}\rho\mathbf{F}. \quad (15)$$

Note that $\mathbf{F}$ also contains the velocity. Equation (15) is a nonlinear equation for the velocity $\mathbf{u}$. Thanks to the quadratic nature of the equation, the velocity $\mathbf{u}$ can be given explicitly by

$$\mathbf{u}=\frac{\mathbf{v}}{c_0+\sqrt{c_0^2+c_1|\mathbf{v}|}}, \quad (16)$$

where $\mathbf{v}$ is a temporal velocity defined as

$$\rho\mathbf{v}=\sum_i \mathbf{e}_i f_i+\frac{\delta_t}{2}\epsilon\rho\mathbf{G}. \quad (17)$$

The two parameters c_0 and c_1 are given by

$$c_0=\frac{1}{2}\left(1+\epsilon\frac{\delta_t}{2}\frac{\nu}{K}\right),\quad c_1=\epsilon\frac{\delta_t}{2}\frac{F_\epsilon}{\sqrt{K}}. \tag{18}$$

Following the approach in Ref. [25], we can obtain the following macroscopic equations from the LBE (13):

$$\frac{\partial\rho}{\partial t}+\nabla\cdot(\rho\mathbf{u})=0, \tag{19a}$$

$$\frac{\partial(\rho\mathbf{u})}{\partial t}+\nabla\cdot\left(\frac{\rho\mathbf{u}\mathbf{u}}{\epsilon}\right)=-\nabla p+\nabla\cdot[\rho\nu_e(\nabla\mathbf{u}+\mathbf{u}\nabla)]+\mathbf{F}, \tag{19b}$$

where the velocity is given by Eq. (16). In the incompressible limit, Eqs. (19) reduce to the generalized Navier-Stokes equations (1). By now, we have derived a generalized lattice Boltzmann equation (GLBE) for flows in porous media. It is noted that as $\epsilon=1$, the GLBE reduces to the standard LBE for flows in the absence of porous media.

If we set $F_\epsilon=0$ in the present model, we can obtain a simplified lattice Boltzmann equation (SLBE) for the Brinkman-extended Darcy model. Note that this simplified model is different from the SP model [20] and the improved version [23] in several ways, although they all use a force term to represent the presence of the porous medium. First, in the present simplified model, the force is included into the LBE based on the method proposed by Guo *et al.* [25], which can produce correct hydrodynamics. But in the original SP model, the force is introduced based on the method of Shan and Chen [29]. However, this approach produces errors of order $\tau^2|\mathbf{F}|^2$ [30]. In the improved SP model [23], the force is included based on the method proposed by Martys *et al.* [30]. However, we have recently shown that this approach also produces undesirable errors [25]. Another difference between the present SLBE and the improved SP model lies in the definitions of the equilibrium distribution functions. In the latter model, the EDF is the same as the one in standard LBM, but in the present SLBE, the porosity of the porous medium is included in the EDF explicitly. These facts indicate that the present GLBE is superior to the original and improved SP models even in the Brinkman limit in theory. What is more important, the two SP models are not suitable for flows with high Reynolds numbers and Darcy numbers, as indicated by Eq. (6).

IV. NUMERICAL RESULTS

To validate the present lattice Boltzmann model, we applied it to three 2D problems: the generalized Poiseuille flow driven by a constant force, the plane Couette flow between two parallel plates, and the lid-driven flow in a square cavity. Since no analytical solutions are available for these problems, the simulation results are compared with the analytical and/or finite-difference solutions for each problem. In our simulations, unless otherwise noted the viscosity ratio is assumed to be unity.

A. Poiseuille flow

We first apply the GLBE to the Poiseuille flow in a 2D channel of width H filled with a porous medium of porosity ϵ. The flow is driven by a constant force G along the channel direction. As the flow is fully developed along the channel, the streamwise velocity (x-direction) satisfies the following equation:

$$\frac{\nu_e}{\epsilon}\frac{\partial^2 u}{\partial y^2}+G-\frac{\nu}{K}u-\frac{F_\epsilon}{\sqrt{K}}u^2=0, \tag{20}$$

with $u(x,0)=u(x,H)=0$, and the lateral velocity component v is zero everywhere.

The Reynolds number of the Poiseuille flow is defined by $\mathrm{Re}=Hu_0/\nu$, where u_0 is the peak velocity of the flow along the centerline in the Brinkman model (see below) given by

$$u_0=\frac{GK}{\nu}\left[1-\cosh^{-1}\left(\frac{rH}{2}\right)\right], \tag{21}$$

where $r=\sqrt{\nu\epsilon/K\nu_e}$.

In simulations, the porosity is set to be 0.1, Re changes from 0.01 to 100, and Da changes from 10^{-6} to 10^2. The lattice used is a 80×80 square mesh, and the relaxation time is set to be 0.8. Periodic boundary conditions are applied to the entrance and the exit, and the nonequilibrium extrapolation scheme [31] is applied to the top and bottom walls for no-slip boundary condition. The velocity field is initialized to be zero at each lattice node with a constant density $\rho=1.0$, and the distribution function is set to be its equilibrium at $t=0$. We first tested the velocity profiles for different values of Re and Da. It is found that as the flow reaches the steady state, the streamwise velocity component u is uniform along the channel, and another velocity component v is of order $O(10^{-12})$ over the whole field. Note that Eq. (20) is a nonlinear equation and it is difficult to obtain the analytical solution. Instead, we solved it using a second-order finite-difference scheme with a uniform mesh of size 1000 in the y direction, and the boundary condition is specified as $u(x,0)=u(x,H)=0$. In Fig. 1 the numerical results of the present lattice Boltzmann model are compared with the finite-difference results. Excellent agreement can be observed between the LBM results and the finite-difference solutions, which confirms the validity of the present LBM.

The nonlinear inertial effect due to the porous medium (Forchheimer term) is also studied. In the absence of this term, the flow at steady state is described by the following Brinkman-extended Darcy equation:

$$\frac{\nu_e}{\epsilon}\frac{\partial^2 u}{\partial y^2}+G-\frac{\nu}{K}u=0. \tag{22}$$

The analytical solution of Eq. (22) can be written as

$$u=\frac{GK}{\nu}\left(1-\frac{\cosh[r(y-H/2)]}{\cosh(rH/2)}\right), \tag{23}$$

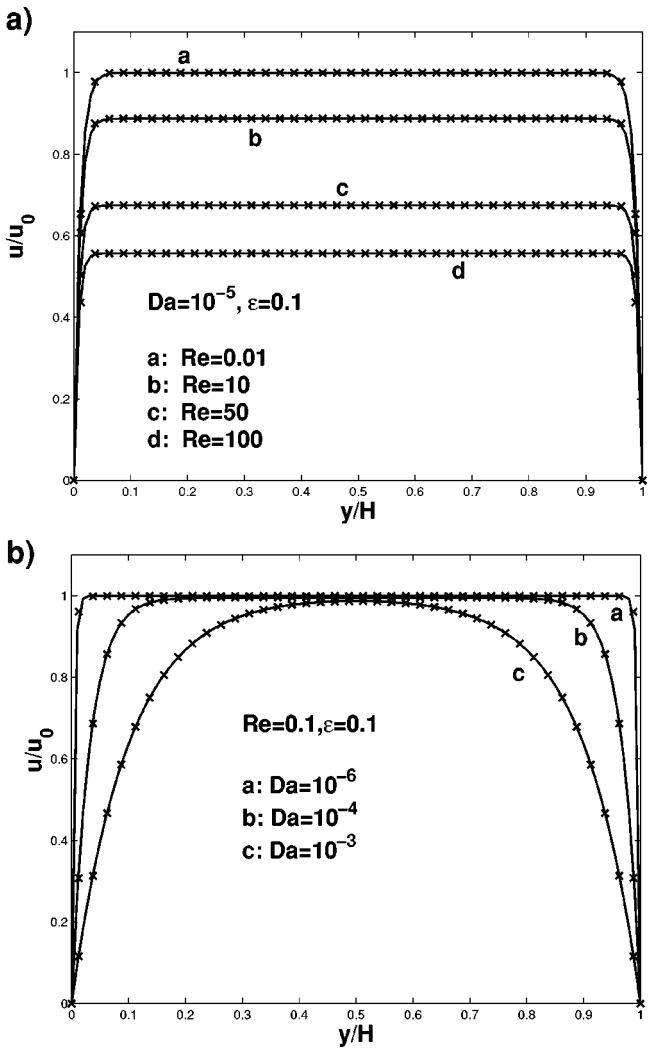

FIG. 1. Velocity profiles of the generalized Poiseuille flow for different Reynolds and Darcy numbers. Symbols represent GLBE solutions and solid lines represent finite-difference solutions.

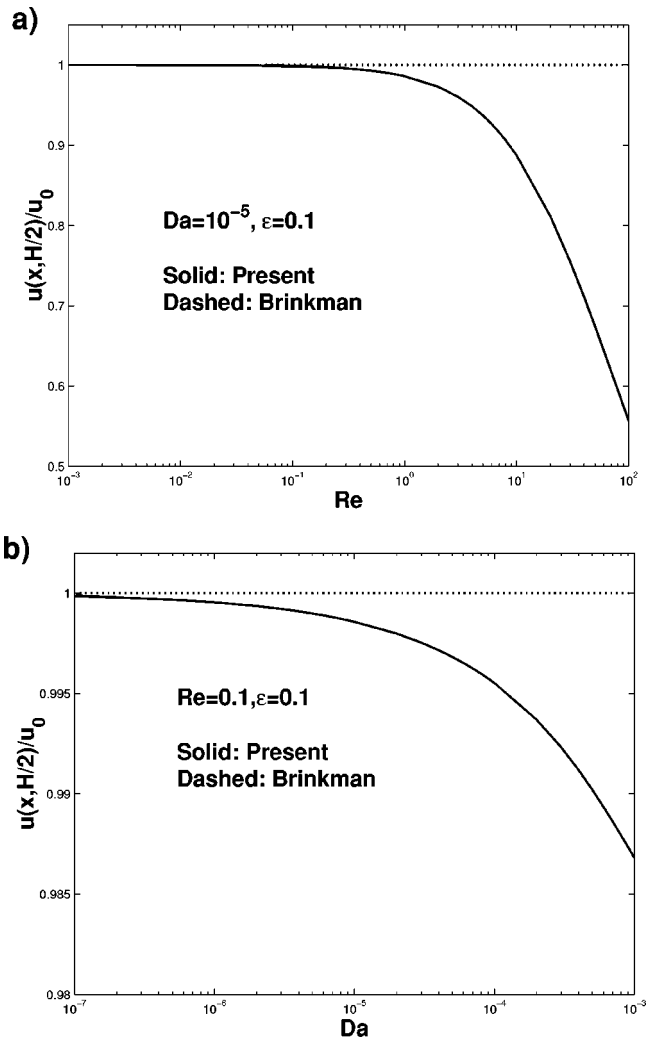

FIG. 2. Peak velocity of the generalized Couette flow for different Reynolds and Darcy numbers.

where $r=\sqrt{\nu\epsilon/K\nu_e}$. As has been pointed in Sec. II, as the Reynolds number or the Darcy number is large, the nonlinear inertial resistance must be considered. In Fig. 2, the peak velocity of the flow is plotted, respectively, against the Reynolds number and the Darcy number. The dashed lines in the figure represent the results from the SLBE for the Brinkman-extended Darcy equation, while the solid lines are the present LBM results for the generalized equation. As can be seen from Fig. 2(a), for a fixed Darcy number (10^{-5}), the effect of the nonlinear drag becomes more pronounced with an increase in Re. Specifically, the results indicate that, the effect of the nonlinear drag is negligible for $\mathrm{Re}\leqslant 0.1$. When $\mathrm{Re}>0.1$, however, the effect of the nonlinear drag becomes significant and increases nearly exponentially with Re. Similarly, Fig. 2(b) also indicates that for a fixed Reynolds number ($\mathrm{Re}=0.1$), the effect of the nonlinear drag becomes more significant with an increase in Da.

B. Couette flow

The Couette flow is also a channel flow similar to the Poiseuille flow, but the flow is now driven by the upper plate moving along the x direction with a constant velocity u_0 instead of a constant force. The Reynolds number of this generalized Couette flow is defined by $\mathrm{Re}=Hu_0/\nu$. At steady state, the flow still obeys Eq. (20), but with $u(x,0)=0$, $u(x,H)=u_0$. Then this one-dimensional ordinary equation is solved with a second-order finite-difference scheme with a uniform mesh of size 1000, and the finite-difference solution will serve as an ''exact solution'' for comparisons. The present GLBE is applied to this Couette flow for different Reynolds and Darcy numbers. The computations are based on a 80×80 lattice in all cases, and the initial and boundary conditions are the same as used in the Poiseuille flow. In Fig. 3, the LBM velocity profiles, together with the finite-difference solutions, are plotted as a function of Re and Da. Good agreement is found between the LBM and the finite-difference solutions.

To study the effect of the nonlinear drag force, we applied both the GLBE and SLBE to this Couette flow at $\mathrm{Re}=10$ for various values of Da. In the case of $F_\epsilon=0$, the Couette flow has the following analytical solution:

$$u=u_0\frac{\sinh(ry)}{\sinh(rH)}, \tag{24}$$

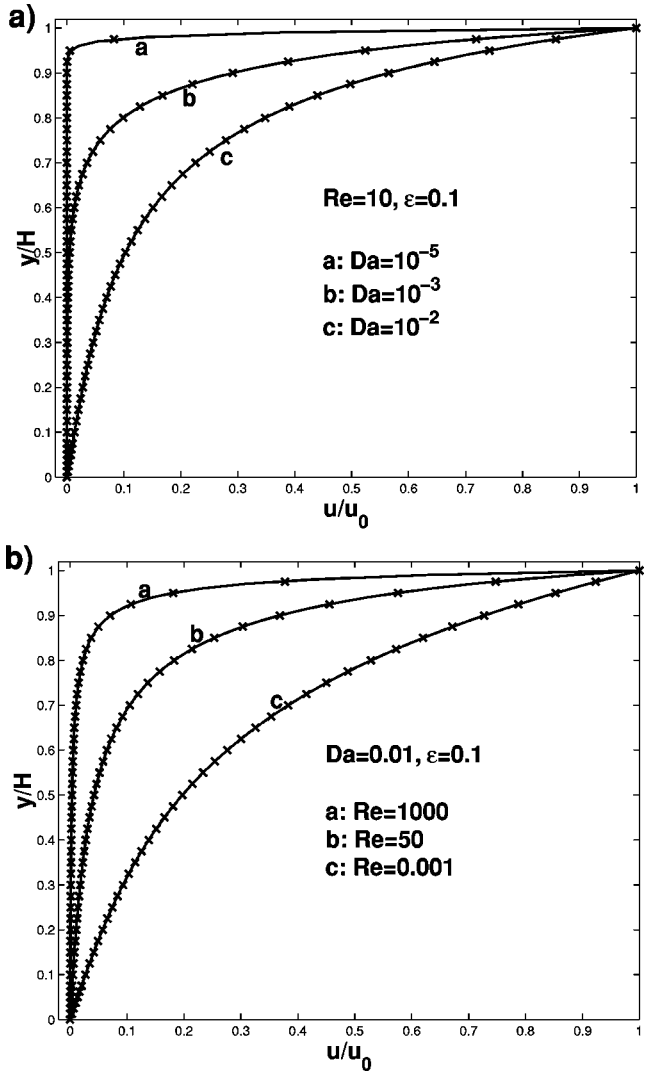

FIG. 3. Velocity profiles of the generalized Couette flow for different Reynolds and Darcy numbers. Symbols represent GLBE solutions and solid lines represent finite-difference solutions.

where $r=\sqrt{\nu\epsilon/K\nu_e}$. In Fig. 4(a), the velocity profiles from the SLBE are present. For comparison, the GLBE results are also shown. One can observe that the SLBE solutions agree well with the analytical solution (24) in the Brinkman limit. To further demonstrate the nonlinear drag effect, the value of the velocity at the midway of channel is measured for different values of Re and Da. $u(x,H/2)/u_0$ against the Darcy number and the Reynolds number are drawn in Figs. 4(b) and 4(c), respectively. From the figure, we can see that the nonlinear drag effect increases both with the Darcy number and the Reynolds number. For small Da and/or Re, the GLBE and SLBE produce almost identical results. But as Da or Re increases, the nonlinear drag force hinders the flow greatly, and it should not be neglected any more.

We also applied the GLBE to a modified Couette flow where a permeable medium is positioned in the channel such that there is a gap between the medium and the upper wall. The porosity is set to be 0.1 for $0\leqslant y\leqslant H/2$ and 1.0 for $H/2<y\leqslant H$. As Re and Da are small, the nonlinear drag

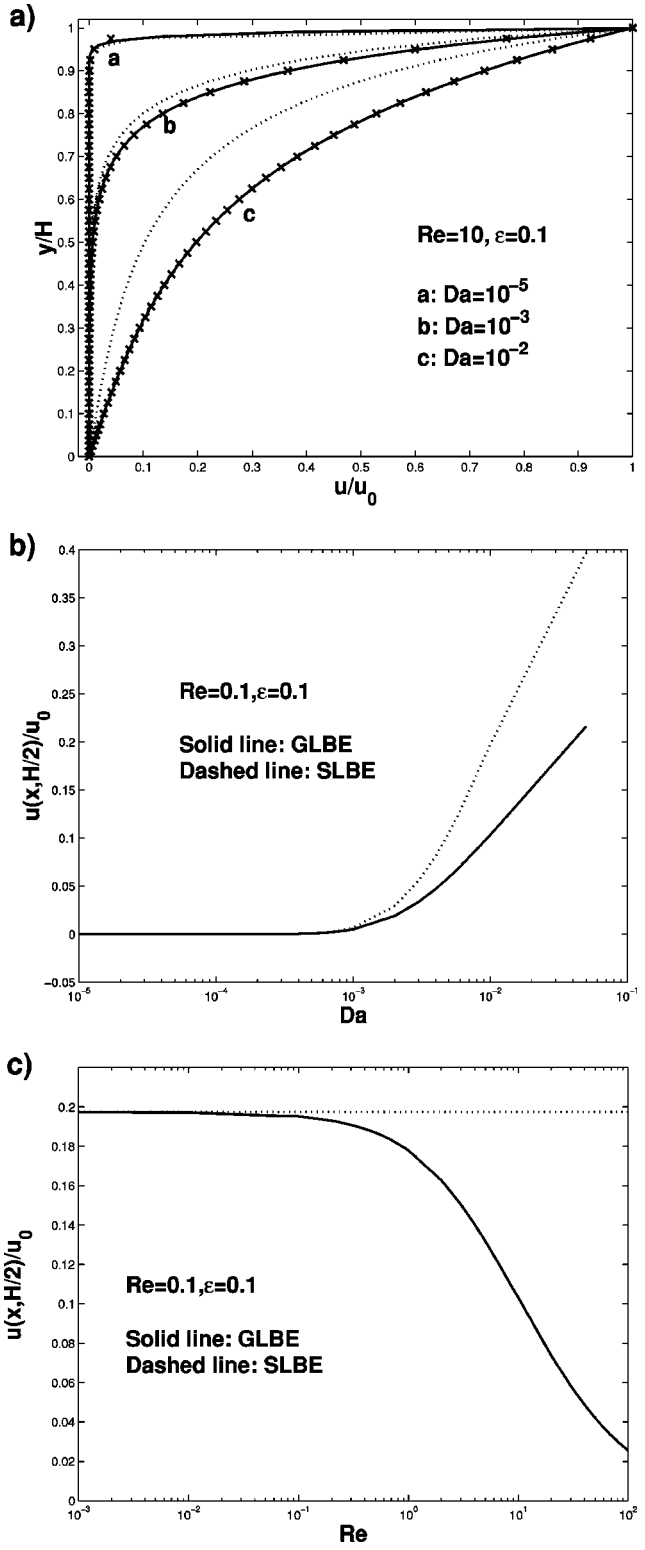

FIG. 4. (a) Velocity profiles of the Couette flow against Reynolds number. The symbol $\times$ represents the SLBE result, the solid line represents analytical solution from Eq. (24), and the dashed line represents GLBE result. (b) Velocity at the midway of the center against Darcy number. (c) Velocity at the midway of the center against Reynolds number.

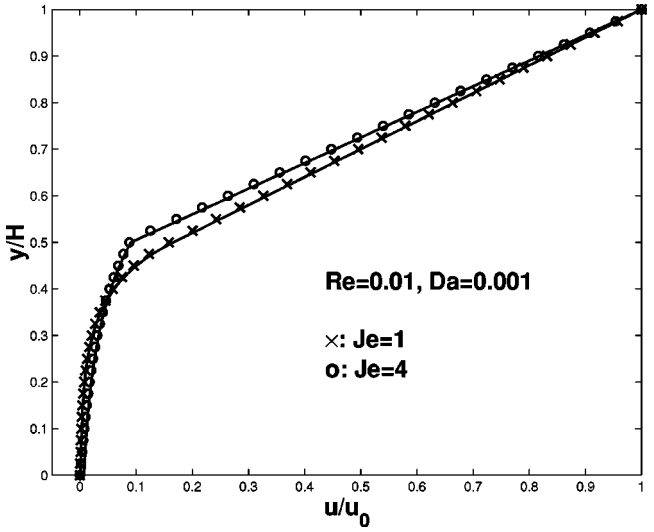

FIG. 5. Velocity profiles of the Couette flow for different viscosity ratios. Solid lines are the approximate analytical solutions from Eq. (25).

effect is negligible, and the velocity can be predicted by the Brinkman equation. It has been shown that the velocity profile is linear in the gap, and exponentially decaying in the porous medium [32]:

$$u = a + b(y/H - 1/2) \quad (H/2 < y \leqslant H),$$

$$u = a \exp(r(y/H - 1/2) \quad (0 \leqslant y \leqslant H/2), \tag{25}$$

where $r = \sqrt{\epsilon\nu/(K\nu_e)}$, $a = 2rKu_0/(2rK+\epsilon)$, and $b = 2\epsilon u_0/(2rK+\epsilon)$. In Fig. 5, velocity profiles are plotted for $J=1$ and 4 at Re$=0.01$ and Da$=0.001$. The good agreement between the simulation and analytical solutions is clearly shown. The GLBE correctly captured the discontinuity of the velocity gradient at the interface without incorporating the stress boundary condition in simulations.

C. Lid-driven cavity flow

The lid-driven cavity flow without porous medium has been used as a benchmarking problem for many numerical methods due to the simple geometry and complicated flow behaviors. In this section we apply the GLBE to the fluid flow in a square cavity of height H filled with a porous medium. The left, right, and bottom walls of the cavity are fixed, and the upper wall moves from left to right with a constant velocity u_0. The nonequilibrium extrapolation scheme [31] is again applied to the four walls for velocity boundary conditions, and the flow field is initialized by setting $\rho = 1.0$ and $\mathbf{u} = 0$.

It is known that as $\epsilon \to 1$, the generalized Navier-Stokes equation will reduce to the standard Navier-Stokes equation. We will first apply the GLBE to the cavity flow in this case to verify it. In simulations, we set Da$=10^4$ and Re$=400$ and 1000. The lattice size is fixed at 128×128. The relaxation time is set to be 0.5174 and 0.5263 for Re$=400$ and 1000, respectively. In Fig. 6, the velocity profiles through the cavity center are plotted. The benchmark solutions of Ref. [33] are also included for comparison. One can see that the GLBE solutions agree well with the benchmark solutions for the cases considered.

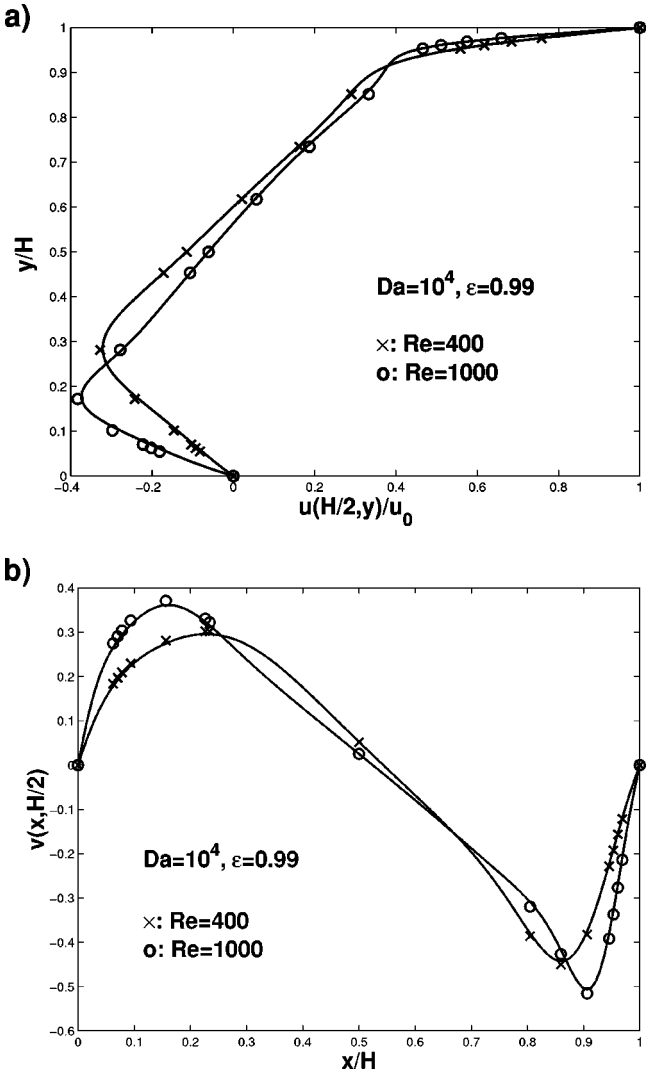

FIG. 6. Velocity profiles through the cavity center. Solid lines are GLBE solutions, and symbols are benchmark solutions in Ref. [33]. (a) u component along the vertical line through the cavity center. (b) v component along the horizontal line through the cavity center.

The GLBE is also applied to the cavity flow with small values of ϵ and Da ($\epsilon = 0.1$, Re$=10$). In Fig. 7, the velocity profiles through the cavity center are plotted for different Darcy numbers. For comparison, the flow is also solved by a finite-difference scheme based on a 256×256 mesh. Clearly, the LBE solutions agree well with the finite-difference solutions for these cases. It is also seen that as Da decreases, the boundary layer near the moving lid becomes thinner, and the vortex in the cavity becomes weaker.

V. SUMMARY

In this paper a lattice Boltzmann model has been proposed for incompressible fluid flows in porous media. The influence of the porous medium is incorporated into the

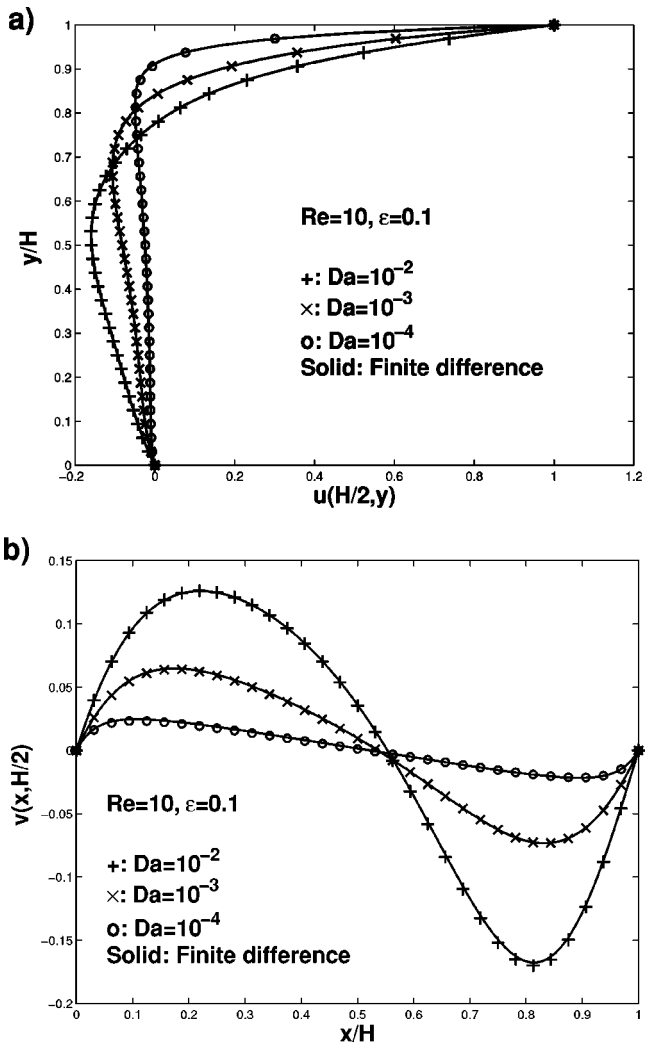

FIG. 7. Velocity profiles through the cavity center. Symbols represent GLBE solutions and solid lines represent finite-difference solutions. (a) u component along the vertical line through the cavity center. (b) v component along the horizontal line through the cavity center.

model by introducing a newly defined equilibrium distribution and adding a force term into the LBE. In the present model, both the linear and the nonlinear drag effects of the medium are considered, and it is applicable to porous flows over a wide range. Another attractive feature of the present model is its ability to model automatically the interfaces between different media without invoking any additional boundary conditions. This feature enables the present LBE more useful in simulating flows in a medium with a variable porosity. Furthermore, the present model is very close to the standard LBM: a simple equilibrium distribution with a simple force term. Therefore, its advantages (e.g., computation efficiency, parallism, and capability to handle interfaces between different fluids) over the solvers for the generalized Navier-Stokes equations are just as those of the standard LBM over the solvers for the Navier-Stokes equations. Furthermore, the interaction between the fluid and the medium is modeled by the force term in the present model. This is, in fact, equivalent to implement an effective boundary condition between the fluid and the solid, like the model proposed in Ref. [19]. From this point of view, one perhaps can directly deduce the drag force due to the porous medium from the boundary rule which is used in the LBM at pore scale, and thus the connection between the LBMs at both the pore and the REV scale is built up. This needs further study and is beyond the present study.

Numerical simulations of several 2D generalized Poiseuille flow, Couette flow, and lid-driven cavity flow have been carried out to validate the present model. It is observed that the present model produces satisfactory solutions for these problems compared with the analytical or the finite-difference solutions. Numerical results also indicate that the nonlinear drag force due to the porous media plays an important role for high-speed flows, and it should not be neglected.

Finally, the present model can only be used to isothermal single-phase fluid flows. Extensions for modeling the problems of convective heat transfer and multiphase flow both with and without a phase change will be considered in future studies.

ACKNOWLEDGMENT

This work was supported by the Hong Kong RGC Earmarked Research Grant No. HKUST 6178/00E.

APPENDIX: DERIVATION OF THE MACROSCOPIC EQUATIONS FROM THE LBE

In this appendix we derive the macroscopic equations from the LBE (9). The $D2Q9$ model is taken as an example. With the definition of the EDF $f_i^{(eq)}$, one can easily obtain the following moments:

$$\sum_i f_i^{(eq)} = \rho, \tag{A1}$$

$$\sum_i \mathbf{e}_i f_i^{(eq)} = \rho \mathbf{u}, \tag{A2}$$

$$\sum_i \mathbf{e}_{i\alpha}\mathbf{e}_{i\beta} f_i^{(eq)} = c_s^2 \rho + \frac{1}{\epsilon}\rho u_\alpha u_\beta, \tag{A3}$$

$$\sum_i \mathbf{e}_{i\alpha}\mathbf{e}_{i\beta}\mathbf{e}_{i\gamma} f_i^{(eq)} = c_s^2 \rho (u_\alpha \delta_{\beta\gamma} + u_\beta \delta_{\alpha\gamma} + u_\gamma \delta_{\alpha\beta}). \tag{A4}$$

The macrodynamical behavior arising from the LBE (5) can be found from a multiscaling analysis using an expansion parameter λ, which is proportional to the ratio of the lattice spacing to a characteristic macroscopic length. To do so, the following expansions are introduced:

$$f_i = f_i^{(0)} + \lambda f_i^{(1)} + \lambda^2 f_i^{(2)} + \cdots, \tag{A5}$$

$$\frac{\partial}{\partial t} = \lambda \frac{\partial}{\partial t_1} + \lambda^2 \frac{\partial}{\partial t_2}, \quad \nabla = \lambda \nabla_1. \tag{A6}$$

Expanding $f_i(\mathbf{x}+\mathbf{e}_i\delta_t, t+\delta_t)$ in Eq. (9) about $\mathbf{x}$ and t, and applying the above multiscaling expansions to the resulting continuous equation, one can obtain the following equations in the consecutive order of the parameter λ:

$$O(\lambda^0):\ f_i^{(0)} = f_i^{(eq)}, \tag{A7}$$

$$O(\lambda^1):\ D_{1i} f_i^{(0)} = -\frac{f_i^{(1)}}{\tau \Delta t}, \tag{A8}$$

$$O(\lambda^2):\ \frac{\partial f_i^{(0)}}{\partial t_2} + \left(1 - \frac{1}{2\tau}\right) D_{1i} f_i^{(1)} = -\frac{f_i^{(2)}}{\tau \Delta t}, \tag{A9}$$

where $D_{1i} = \frac{\partial}{\partial t_1} + \mathbf{e}_i \cdot \boldsymbol{\nabla}_1$.

Note that from the definitions of ρ and $\mathbf{u}$ [Eq. (11)] and the moment equations Eqs. (A1) and (A2), one can obtain that

$$\sum_i f_i^{(k)} = 0, \quad \sum_i \mathbf{e}_i f_i^{(k)} = \mathbf{0} \quad \text{for } k \geqslant 1. \tag{A10}$$

Taking moments of Eq. (A8), we can obtain the macroscopic equations on the $t_1 = \epsilon t$ time scale and $\mathbf{x}_1 = \epsilon \mathbf{x}$ space scale:

$$\frac{\partial \rho}{\partial t_1} + \boldsymbol{\nabla}_1 \cdot (\rho \mathbf{u}) = 0, \tag{A11a}$$

$$\frac{\partial (\rho \mathbf{u})}{\partial t_1} + \boldsymbol{\nabla}_1 \cdot \Pi^{(0)} = \mathbf{0}, \tag{A11b}$$

where $\Pi^{(0)}$ is the zeroth-order momentum flux tensor given by $\Pi^{(0)}_{\alpha\beta} = \Sigma_i \mathbf{e}_{i\alpha} \mathbf{e}_{i\beta} f_i^{(0)} = c_s^2 \rho \delta_{\alpha\beta} + \rho \mathbf{u}_\alpha \mathbf{u}_\beta / \epsilon$. The first-order momentum flux $\Pi^{(1)} \equiv \Sigma_i \mathbf{e}_i \mathbf{e}_i f_i^{(1)}$ can be simplified using Eqs. (A11). After some standard algebra, we obtain that

$$\Pi^{(1)}_{\alpha\beta} = -c_s^2 \tau \delta_t \rho (\boldsymbol{\nabla}_{1\alpha} \mathbf{u}_\beta + \boldsymbol{\nabla}_{1\beta} \mathbf{u}_\alpha), \tag{A12}$$

where the terms of order $O(M^3)$ have been neglected. Here $M = u/c_s$ is the Mach number.

The macroscopic equations on the $t_2 = \lambda^2 t$ time scale are derived by taking moments of Eq. (A9). With the aid of Eqs. (A11), the final equations can be written as

$$\frac{\partial \rho}{\partial t_2} = 0, \tag{A13a}$$

$$\frac{\partial (\rho \mathbf{u})}{\partial t_2} = \boldsymbol{\nabla}_1 \cdot [\rho \nu_e (\boldsymbol{\nabla}_1 \mathbf{u} + \mathbf{u} \boldsymbol{\nabla}_1)], \tag{A13b}$$

where

$$\nu_e = \left(\tau - \frac{1}{2}\right) c_s^2 \delta_t. \tag{A14}$$

Combining the macroscopic equations on the t_1 and t_2 scales, one finally obtains macroscopic equations given by Eq. (12).

[1] C.L. Tien and K. Vafai, Adv. Appl. Mech. **27**, 225 (1990).
[2] C.T. Hsu and P. Cheng, Int. J. Heat Mass Transf. **33**, 1587 (1990).
[3] P. Nithiarasu, K.N. Seetharamu, and T. Sundararajan, Int. J. Heat Mass Transf. **40**, 3955 (1997).
[4] C.E. Hickox and D.K. Gartling, Int. J. Heat Mass Transf. **28**, 720 (1985).
[5] T. Nishimura *et al.*, Int. J. Heat Mass Transf. **29**, 889 (1986).
[6] D.K. Gartling, C.E. Hickox, and R.C. Givler, Theor. Comput. Fluid Dyn. **7**, 23 (1996).
[7] P. Nithiarasu and K. Ravindran, Comput. Methods Appl. Mech. Eng. **165**, 147 (1998).
[8] A. Amiri, Int. J. Heat Mass Transf. **43**, 3513 (2000).
[9] S. Chen and G.D. Doolen, Annu. Rev. Fluid Mech. **30**, 329 (1998).
[10] K. Balasubramanian, F. Hayot, and W.F. Saam, Phys. Rev. A **36**, 2248 (1987).
[11] D.H. Rothman, Geophysics **53**, 509 (1988).
[12] S. Succi, E. Foti, and F. Higuera, Europhys. Lett. **10**, 433 (1989).
[13] A. Adrover and M. Giona, Chem. Eng. J. **64**, 7 (1996).
[14] A. Koponen, M. Kataja, and J. Timonen, Int. J. Mod. Phys. C **9**, 1505 (1998).
[15] K. Langass and D. Grubert, J. Pet. Sci. Eng. **24**, 199 (1999).
[16] M. Singh and K.K. Mohanty, Chem. Eng. Sci. **55**, 5393 (2000).
[17] J. Bernsdorf, G. Bernner, and F. Durst, Comput. Phys. Commun. **129**, 247 (2000).
[18] J. Kim, J. Lee, and K.-C. Lee, Physica A **293**, 13 (2001).
[19] O. Dardis and J. McCloskey, Phys. Rev. E **57**, 4834 (1998).
[20] M.A.A. Spaid and F.R. Phelan, Jr., Phys. Fluids **9**, 2468 (1997).
[21] D.M. Freed, Int. J. Mod. Phys. C **9**, 1491 (1998).
[22] M.A.A. Spaid and F.R. Phelan, Jr., Composites, Part A **29A**, 749 (1998).
[23] N.S. Martys, Phys. Fluids **6**, 1807 (2001).
[24] K. Vafai and S.J. Kim, Int. J. Heat Fluid Flow **16**, 11 (1995).
[25] Z. Guo, C. Zheng, and B. Shi, Phys. Rev. E **65**, 046308 (2002).
[26] S. Ergun, Chem. Eng. Prog. **48**, 89 (1952).
[27] K. Vafai, J. Fluid Mech. **147**, 233 (1984).
[28] Y. Qian, D. d'Humiéres, and P. Lallemand, Europhys. Lett. **17**, 479 (1992).
[29] X. Shan and H. Chen, Phys. Rev. E **47**, 1815 (1993).
[30] N.S. Martys, X. Shan, and H. Chen, Phys. Rev. E **58**, 6855 (1998).
[31] Z. Guo, C. Zheng, and B. Shi, Phys. Fluids **14**, 2007 (2002).
[32] N.S. Martys, D.B. Bentz, and E.J. Garboczi, Phys. Fluids **6**, 1434 (1994).
[33] U. Ghia, K.N. Ghia, and C.T. Shin, J. Comput. Phys. **48**, 387 (1982).